ARCHIVES OF ELECTRICAL ENGINEERING VOL. 59(1-2), pp. 35-49 (2010)

DOI 10.2478/s10171-010-0003-2

Discharge channel displacement simulation in AC arc

TOMASZ DASZKIEWICZ, WITOLD TARCZYŃSKI

Department of Electrical Apparatus, Technical University of Lodz
B. Stefanowskiego 18/22, 90-924 Łódź, Poland
e-mail: wtarczyn@p.lodz.pl, tdaszek@p.lodz.pl

(Received: 06.11.2009, revised: 01.12.2009)

Abstract: Results of 3-D of discharge channel displacement simulation, acquired by means of the Fluent program during one current half-period of AC arc, indicate that the obtained images of the phenomenon are qualitatively similar to those, recorded with a high-speed digital camera, while the computer simulation enables much a more comprehensive analysis of the acquired data. In addition to selected arc simulation frames and corresponding distributions of mass velocity vectors and current density vectors on a plane, the distributions of temperature, current density and mass velocity values are presented on the axis of the electrode arrangement model. The composite motion (continuous and jumping) of discharge channels was analyzed, taking into account mass displacement and matter state changes.

Key words: switching arcs, arc motion velocity, computer AC arc simulation

1. Introduction

Switching arc is a very complex phenomenon, particularly in cases where the whole burning process of a high-current arc should be taken into account, simultaneously on contacts, arc runners, and in the extinguishing chamber. Therefore, a number simplifications were employed in arc motion simulation, dividing the process into selected time intervals, simplifying the contact-extinguishing system, etc. For many years, researchers, involved in switch arc investigations, were intuitively inclined to perceive arc motion as hot matter motion. Even in the last years, switch arc motion was simulated as the motion of a massive rod [1, 2], the geometry of which was determined mostly from photographic images. The parameters of motion (velocity and path) were derived from mass motion equations, assuming drag coefficients to be characteristic for massive rods or determined by experiments. Due to the high switch arc burning dynamics and turbulent phenomena and depending on test conditions, various drag coefficients were derived for static conditions (direct current), being even more complicated when alternate current switch arc was investigated and the drag coefficient variations followed current half-periods [3-6]. The problem is still more involved when arc-backs, as observed in electric switches, are analyzed, i.e. arc returns in contact-extinguishing systems or between

plasma jets [4, 7, 8]. An abrupt arc displacement can occur not only in reverse but in forward direction as well. Thus, it is rather difficult to apply a massive rod model for the simulation of the whole arc motion process during switch current breaking.

Arc motion modeling complexity was for the first time more broadly approached by Maecker [9, 10], who distinguished three arc motion velocities. The first one $(\vec{v}_A)$ results from the fact that electric arc appears as a luminous phenomenon, temperature cloud being the source of generated light. In a temperature cloud, in contrast to a mass cloud, new amount quantities can be created in each maximum by temperature elevation. Maecker, taking into account the difficulties with determining the parameters of that cloud, proposed a simplified solution, defining the position as that of temperature maximum (symbols with m index), and arc motion (symbols with index *A*) as that of temperature maximum:

$$\vec{r}_A = \vec{r}_m, \quad \vec{v}_A = \vec{v}_m \ . \tag{1}$$

Then, the arc motion equation is, by definition:

$$\nabla_{m0} \frac{\partial T}{\partial t} = -\left(\vec{v}_A \cdot \nabla_{m0}\right) \nabla T \ . \tag{2}$$

This equation can be interpreted as a phenomenological equation, according to which the gradient of temperature variation in time, i.e., heating heterogeneity in the maximum causes arc motion and the $[(\nabla_{m0})\nabla T]^{-1}$ operator plays the role of coefficient. Maecker mentions a stretched wire with ohmic heating, with its temperature maximum located in the middle between clamps, as the simplest example to explain the equation. If this wire is submitted to non uniform heating around its temperature maximum, so that one side of the maximum is heated, while the other is cooled, the temperature maximum will move towards heating side. A uniform heating of both sides of the maximum would raise the wire temperature, not shifting the maximum though. For this simple linear example the velocity of the temperature maximum can be determined, according to (2) and resulting in:

$$v_A = \frac{\left(\dfrac{-\partial^2 T}{\partial x \partial t}\right)_m}{\left(\dfrac{\partial^2 T}{\partial x^2}\right)_m} \ . \tag{3}$$

The other two velocities include $\vec{v}_M$ velocity, the source of which are either external forces or a pressure gradient, and the relative velocity of arc and matter $(\vec{v}_{AM})$. Maecker gives a few arc motion examples for three different cases:

- no mass flow $\vec{v}_M$, and arc motion induced by various heterogeneous heating modes,
- no arc motion $\vec{v}_A$, correspondingly to the dynamic equilibrium of $\vec{v}_{AM} = -\vec{v}_M$,
- no relative motion between the arc and matter $\vec{v}_{AM}$.

The arc position was in Maecker's considerations defined as the temperature maximum.

Engineers and research workers have two possible ways to approach the problem of arc motion modeling and simulation – a design of their own models and development of the, so-called, home program codes or the use of commercially available software packages. Home codes were very widely applied for the investigations of characteristic physical properties, parametric investigations or for evaluation of the influence of a given parameter on simplified geometry. As it has been mentioned above, an arc model in a form of massive rod was then used or more complicated programs were developed, associated with a combined analysis of electromagnetic and aerothermodynamic phenomena [11, 12]. As the years went by, the data processing potentials of computers were getting higher and computer packages were becoming more and more professional. Therefore, the derived models could approximate the real geometry of investigated objects and making possible calculations for 2-D and 3-D models [13-25]. For plasma modeling, various commercial software packages are now applied (for example: Phoenics, Fluent, Flow3D, Estet, and so on). For modeling and simulation of plasma flows in electrical devices, the Fluent package has gained much popularity in the recent years. The authors of this article have mainly been involved in the investigations of systems that are characteristic for switches. The publications [21, 24, 25] should be mentioned in this field.

This article presents modeling and simulation for an arrangement of plasma jets with a discharge channel between them, which is characteristic for a high-current switch arc described in [8], where results of experimental investigations are presented, supported by the use of high-speed digital cameras.

2. Arc model

The phenomenon of discharge channel displacement in AC free-burning arc in the air, investigated experimentally [7] and described widely [8], was modeled, using the electrode arrangement as shown in Fig. 1.

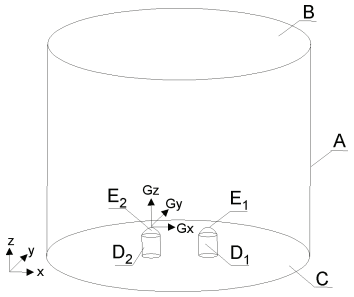

Fig. 1. Modeled arrangement of parallel electrodes. A, B, C – surfaces determining the limit surfaces; E_1, E_2 – surfaces of electrode tips, D_1, D_2 – lateral surfaces of the electrodes

The modeling and simulation of the investigated phenomenon was carried out with the Fluent program. Using the program, a system of magnetohydrodynamic equations can be solved by connecting electromagnetic field equations with Navier-Stokes flow equations in control volume.

Additional equations, which take account of the presence of electromagnetic field, having the form of subroutines, self-developed by the user (user-defined scalars), were appended to the general transportation equations, which are solved by the Fluent program, such as the equations of mass, energy and momentum conservation. In order to consider a current flow field in arc, it is necessary to include additional heat sources into the equations of momentum and energy conservation, that is Joule heat, as well as energy losses, associated with radiation from the arc core. The component of Lorentz force was also added to the equations of momentum conservation to take account of the self-induction magnetic field.

For the arc model, presented in the 3-D Cartesian coordinate system in non-stationary state, all the equations for the mass, momentum and energy can be written in the form as proposed by Patankar [26]:

$$\underbrace{\frac{\partial}{\partial t}(\rho\phi)}_{\text{time component}} + \underbrace{\vec{\nabla}\cdot(\rho\vec{v}\phi)}_{\text{convection component}} = \underbrace{\vec{\nabla}\cdot\left(\Gamma_\phi\vec{\nabla}\phi\right)}_{\text{diffusion component}} + \underbrace{S_\phi}_{\text{source component}}, \tag{4}$$

$$\frac{\partial\rho\phi}{\partial t} + \frac{\partial}{\partial x}(\rho v_x\phi) + \frac{\partial}{\partial y}(\rho v_y\phi) + \frac{\partial}{\partial_z}(\rho v_z\phi) = \frac{\partial}{\partial x}\left(\Gamma_\phi\frac{\partial\phi}{\partial x}\right) + \frac{\partial}{\partial y}\left(\Gamma_\phi\frac{\partial\phi}{\partial y}\right) + \frac{\partial}{\partial z}\left(\Gamma_\phi\frac{\partial\phi}{\partial z}\right) + S_\phi\,. \tag{5}$$

Table 1 brings together the equations of arc plasma in the 3-D coordinate system. These equations are based on the general formulas for convection and diffusion, as proposed by Patankar. Momentum components include additional factors that reflect arc presence. In equations (4), (5) and Table 1 Γ_ϕ is the diffusion coefficient, S_ϕ is a heat source, and ϕ represents a scalar variable that is successively solved for the equations of energy, momentum and mass conservation. The v_x, v_y and v_z variables are three components of the velocity vector $\vec{v}$, ρ is the fluid mass density, j_x, j_y and j_z variables are the three components of current density vector, B_x, B_y and B_z variables are magnetic field components, calculated from the three potential vector components, μ, k C_p, h, σ, respectively, denote viscosity, thermal conductivity, specific heat, enthalpy and electric conductivity of plasma. The radiation losses can be written as $4\pi\varepsilon_N$, where ε_N is NEC (net emission coefficient).

In order to obtain the equation for the scalar potential in stationary state and to find out components electric current density, it is necessary to solve equation (4) with the following assumptions: the diffusion coefficient is equal to electric conductivity, and the source component is equal to zero:

$$\phi = V,\ \Gamma_\phi = \sigma,\ S_\phi = 0, \tag{6}$$

where: V is the scalar potential.

It was assumed that the convection component was not calculated ($\rho\ v\ \phi$) = 0, thus the equation adopted the following form:

$$\vec{\nabla}\cdot\left(\Gamma_\phi\vec{\nabla}\phi\right) + S_\phi = 0\,. \tag{7}$$

Table 1. Equations of arc plasma in the 3-D coordinate system

Equations for	ϕ	Γ_ϕ	S_ϕ
x – component of the momentum	v_x	μ	$-\frac{\partial p}{\partial x}+\frac{\partial}{\partial y}\mu\left(\frac{\partial v_x}{\partial y}+\frac{\partial v_x}{\partial x}\right)+\frac{\partial}{\partial z}\mu\left(\frac{\partial v_x}{\partial z}+\frac{\partial v_z}{\partial x}\right)+\frac{4}{3}\frac{\partial}{\partial x}\left(\mu\frac{\partial v_x}{\partial y}\right)-\frac{2}{3}\frac{\partial}{\partial x}\mu\left(\frac{\partial v_y}{\partial y}+\frac{\partial v_z}{\partial z}\right)$ $+j_z B_y - j_y B_z$
y – component of the momentum	v_y	μ	$-\frac{\partial p}{\partial x}+\frac{\partial}{\partial z}\mu\left(\frac{\partial v_y}{\partial z}+\frac{\partial v_y}{\partial y}\right)+\frac{\partial}{\partial x}\mu\left(\frac{\partial v_y}{\partial x}+\frac{\partial v_x}{\partial y}\right)+\frac{4}{3}\frac{\partial}{\partial y}\left(\mu\frac{\partial v_y}{\partial y}\right)-\frac{2}{3}\frac{\partial}{\partial y}\mu\left(\frac{\partial v_z}{\partial z}+\frac{\partial v_x}{\partial x}\right)$ $+j_x B_z - j_z B_x$
z – component of the momentum	v_z	μ	$-\frac{\partial p}{\partial x}+\frac{\partial}{\partial x}\mu\left(\frac{\partial v_z}{\partial x}+\frac{\partial v_z}{\partial z}\right)+\frac{\partial}{\partial y}\mu\left(\frac{\partial v_z}{\partial y}+\frac{\partial v_y}{\partial z}\right)+\frac{4}{3}\frac{\partial}{\partial z}\left(\mu\frac{\partial v_z}{\partial z}\right)-\frac{2}{3}\frac{\partial}{\partial z}\mu\left(\frac{\partial v_x}{\partial x}+\frac{\partial v_y}{\partial y}\right)$ $+j_y B_x - j_x B_y$
Energy	h	$\frac{\kappa}{C_p}$	$v_x\frac{\partial p}{\partial x}+v_y\frac{\partial p}{\partial y}+v_z\frac{\partial p}{\partial z}+$ $\mu\left\{2\cdot\left[\left(\frac{\partial v_x}{\partial x}\right)^2+\left(\frac{\partial v_y}{\partial y}\right)^2+\left(\frac{\partial v_z}{\partial z}\right)^2\right]+\left[\frac{\partial v_y}{\partial x}+\frac{\partial v_x}{\partial y}\right]^2+\left[\frac{\partial v_z}{\partial y}+\frac{\partial v_y}{\partial z}\right]^2+\left[\frac{\partial v_x}{\partial z}+\frac{\partial v_z}{\partial x}\right]^2\right.$ $\left.-\frac{2}{3}\cdot\left[\frac{\partial v_x}{\partial x}+\frac{\partial v_y}{\partial y}+\frac{\partial v_z}{\partial z}\right]^2\right\}+$ $+\frac{j_x^2+j_y^2+j_z^2}{\sigma}-4\pi\varepsilon_N+\frac{5}{2}\frac{k}{e}\left(\frac{j_x}{C_p}\frac{\partial h}{\partial x}+\frac{j_y}{C_p}\frac{\partial h}{\partial y}+\frac{j_z}{C_p}\frac{\partial h}{\partial z}\right)$

After substitution of assumptions (6) to the Equation (7), the following result is obtained:

$$-\vec{\nabla}\cdot\left(\sigma\vec{\nabla}V\right)=0\,, \tag{8}$$

$$\frac{\partial}{\partial x_i}\left(-\sigma\frac{\partial V}{\partial x_i}\right)=0\,, \tag{9}$$

$$\frac{\partial}{\partial x_i}\left(-\sigma\,\mathrm{grad}\,V\right)=0\,. \tag{10}$$

Provided that $\frac{\partial}{\partial x_i}$ is the derivative of the vector with respect to spatial variables, it is then possible to write:

$$div\left(-\sigma\,\mathrm{grad}\,V\right)=0\,. \tag{11}$$

Therefore the components of electric current density are the following:

$$j_x = -\sigma \frac{\partial V}{\partial x}, \quad j_y = -\sigma \frac{\partial V}{\partial y}, \quad j_z = -\sigma \frac{\partial V}{\partial z}. \tag{12}$$

In order to obtain solutions for vector potential, it is necessary to solve equation (4), with the following assumptions: the diffusion coefficient equals to 1 and the source component is $\mu_0 \cdot \vec{j}$

$$\phi = \vec{A}, \quad \Gamma_\phi = 1, \quad S_\phi = \mu_0 \cdot \vec{j}, \tag{13}$$

where: $\vec{A}$ is the vector potential, μ_0 is the absolute magnetic permeability of vacuum, $\vec{j}$ is the electric current density vector.

Assuming that the convection component is zero, the following form of equation (4) is obtained:

$$\vec{\nabla} \cdot \left(\Gamma_\phi \vec{\nabla} \phi\right) + S_\phi = 0. \tag{14}$$

After substitution of assumptions (13) into equation (14), Poisson's equation is obtained:

$$\vec{\nabla} \cdot \left(1 \cdot \vec{\nabla} \vec{A}\right) = -\mu_0 \cdot \vec{j}, \tag{15}$$

$$\vec{\nabla}^2 \vec{A} = -\mu_0 \cdot \vec{j}, \tag{16}$$

$$\text{div grad } A_i = -\mu_0 \cdot j_i. \tag{17}$$

Hence, the components of the vector potential can be presented in the following form:

$$A_x = -\mu_0 \cdot j_x, \quad A_y = -\mu_0 \cdot j_y, \quad A_z = -\mu_0 \cdot j_z. \tag{18}$$

Having used the relation $\vec{B} = \text{rot } \vec{A}$, it is possible to find out the components of magnetic induction:

$$B_x = \frac{\partial A_z}{\partial y} - \frac{\partial A_y}{\partial z}, \quad B_y = \frac{\partial A_x}{\partial z} - \frac{\partial A_z}{\partial x}, \quad B_z = \frac{\partial A_y}{\partial x} - \frac{\partial A_x}{\partial y}. \tag{19}$$

Finally, one can conclude that the scalar equations make it possible to incorporate the Maxwell equations to the Fluent program, taking into account the effects of both magnetic and electric fields on arc plasma flow:

$$\text{div}\left(-\sigma \text{ grad } V\right) = 0; \quad \text{div } \vec{E} = 0; \quad \text{div } \vec{B} = 0; \quad \text{rot } \vec{B} = \mu_0 \cdot \vec{j}, \tag{20}$$

where: $\vec{E}$ is the vector of the electric field strength, $\vec{B}$ is the vector of magnetic induction.

Table 2 presents boundary conditions for the system of free-burning arc in the arrangement of parallel electrodes. Surfaces A-E correspond to those in Fig. 1.

Table 2. Boundary conditions for the system of free-burning arc

Surface	P	v_x	v_y	v_z	T	V	A_x	A_y	A_z
A, C	1 *atm*	$\frac{\partial v_x}{\partial \vec{n}} = 0$	$\frac{\partial v_y}{\partial \vec{n}} = 0$	$\frac{\partial v_z}{\partial \vec{n}} = 0$	2500	$\frac{\partial V}{\partial \vec{n}} = 0$	0	0	0
B	1 *atm*	$\frac{\partial v_x}{\partial \vec{n}} = 0$	$\frac{\partial v_y}{\partial \vec{n}} = 0$	$\frac{\partial v_z}{\partial \vec{n}} = 0$	2500	$\frac{\partial V}{\partial \vec{n}} = 0$	0	0	0
E_1	–	0	0	0	3500	$j_z(x,y)$	$\frac{\partial A_x}{\partial \vec{n}} = 0$	$\frac{\partial A_y}{\partial \vec{n}} = 0$	$\frac{\partial A_z}{\partial \vec{n}} = 0$
E_2	–	0	0	0	$\frac{\partial T}{\partial z} = 0$	0	$\frac{\partial A_x}{\partial z} = 0$	$\frac{\partial A_y}{\partial z} = 0$	$\frac{\partial A_z}{\partial z} = 0$
D_1, D_2	–	0	0	0	3500	$\frac{\partial V}{\partial \vec{n}} = 0$	$\frac{\partial A_x}{\partial \vec{n}} = 0$	$\frac{\partial A_y}{\partial \vec{n}} = 0$	$\frac{\partial A_z}{\partial \vec{n}} = 0$

Self-induced magnetic field plays an important role for electric arc behavior, as in combination with electric current density, it increases Lorentz force. In order to calculate the level of magnetic field, one can use two possible options: to compute field parameters from Biot-Savart's law or to use vector potential rotation. The use of Biot-Savart's law to calculate the parameters of magnetic field, induced by electric arc, needs a long computation time. It is why the simulation takes account of the self-inducted magnetic field, computed from the vector potential.

The following distribution of electric current density was adopted at the electrode surface:

$$j_z(x,y) = J_{\max} \cdot \exp\left(-b\sqrt{x^2+y^2}\right) \cdot \sin \omega t, \tag{21}$$

where: $J_{\max} = 1.4 \cdot 10^8\ A/m^2$, b is the constant, x, y is the Cartesian coordinates in the Cartesian system of coordinates, $\omega = 2 \cdot \pi \cdot f$ is the pulsation of the power supply voltage.

3. Test results

Fig. 2 shows the selected frames of computer simulation of AC free-burning electric arc at $I_{\max}$ = 800 A, 50 Hz in the air at atmospheric pressure, for one current half-period. Temperature distributions are shown on the left side with corresponding pictures of current density vectors for respective times t = 2.20 ms, t = 2.64 ms and t = 2.80 ms. The pictures present the successive phases of arc column development and the forming of a new discharge channel between plasma jets. Figure 3 shows temperature distributions and mass velocity vectors for the same time values.

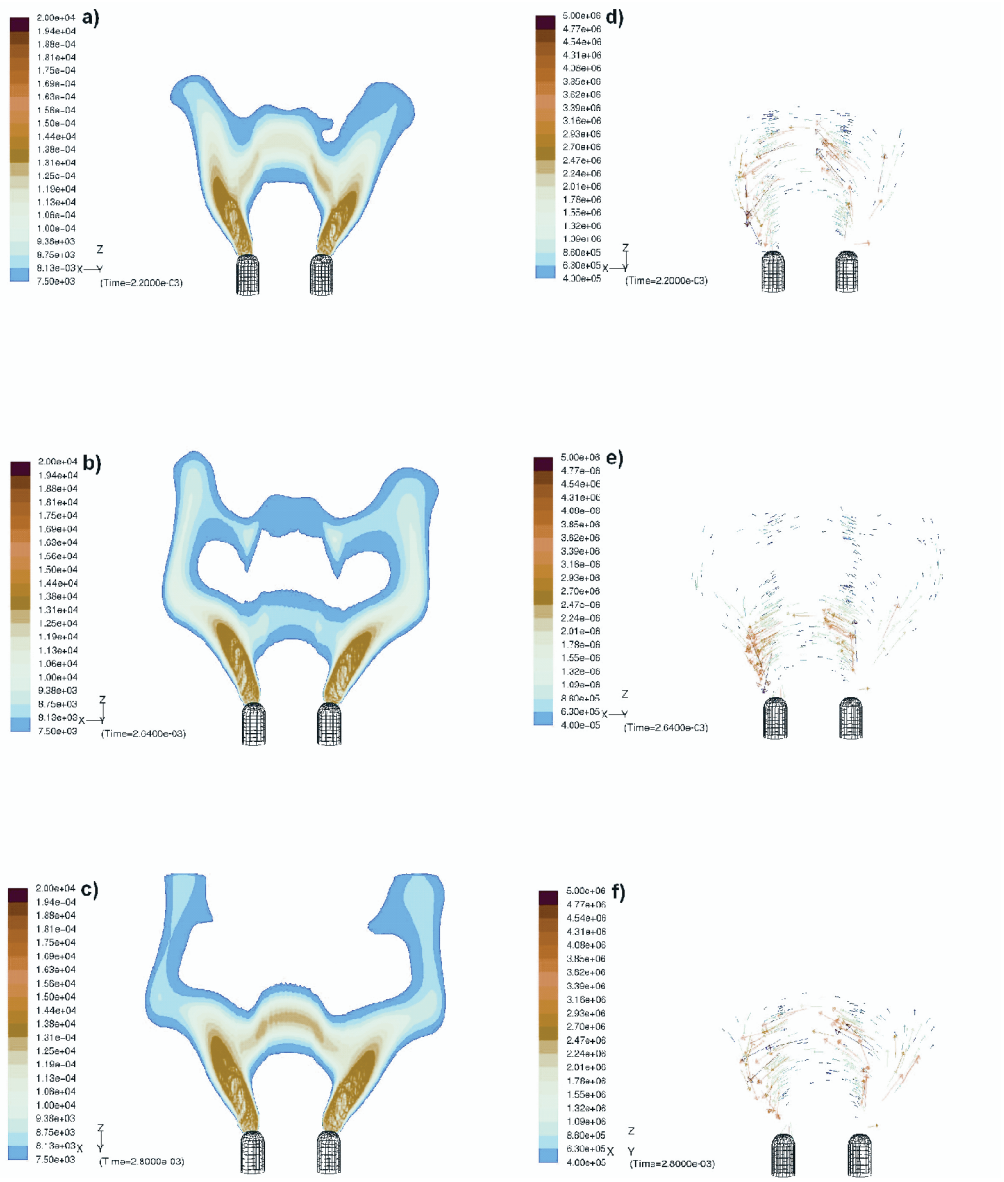

Fig. 2. Selected frames of a computer simulation of AC electric arc at I_{max} = 800 A, burning freely in the air at atmospheric pressure, for one current half-period. Temperature distributions are shown on the left side with the corresponding pictures of current density vectors for successive times t = 2.20 ms, t = 2.64 ms and t = 2.80 ms

It is evident in Fig. 2b that a new discharge channel was formed between plasma jets below the channel, which conducted current a while before (Fig. 2a). It amounts to the appearance of a current in the new channel (shown in Fig. 2e) and the decay of a current flow in the previous channel (Fig. 2d). Therefore, the discharge channel is displaced over here between

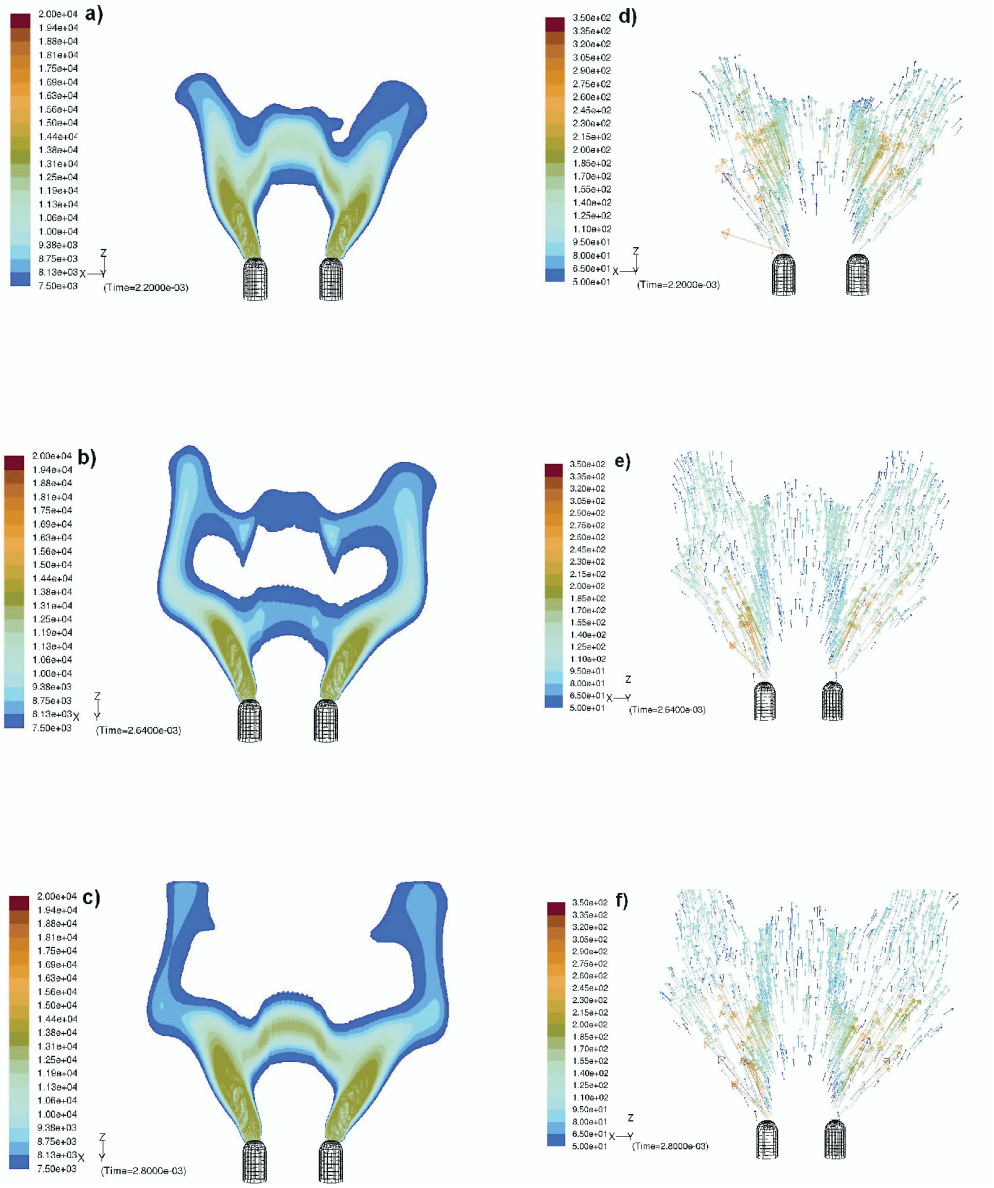

Fig. 3. Selected frames of computer simulation of AC electric arc at I_{max} = 800 A, burning freely in the air at atmospheric pressure, for one current half-period. Temperature distributions are shown on the left side, and next the corresponding pictures of mass velocity vectors at times t = 2.20 ms, t = 2.64 ms and t = 2.80 ms, respectively

plasma jets. The presented displacement of the current channel is not accompanied by the change of mass flow direction (Fig. 3e), which reveals a fact that such jumping displacement of discharge channels in AC arc under present test conditions was associated with matter state changes.

As it results from Figs. 4, 5, the mass is displaced with definite velocity distributions, as well temperature distributions are displaced in time along the axis of the model arrangement (Figs. 6, 7) until the plasma state is modified at any plasma point, for example, until a new discharge channel is formed. Then, one gets an impression from the photographic observations that "a luminous temperature cloud" jumped to the other place but, in fact, it was the plasma state which changed.

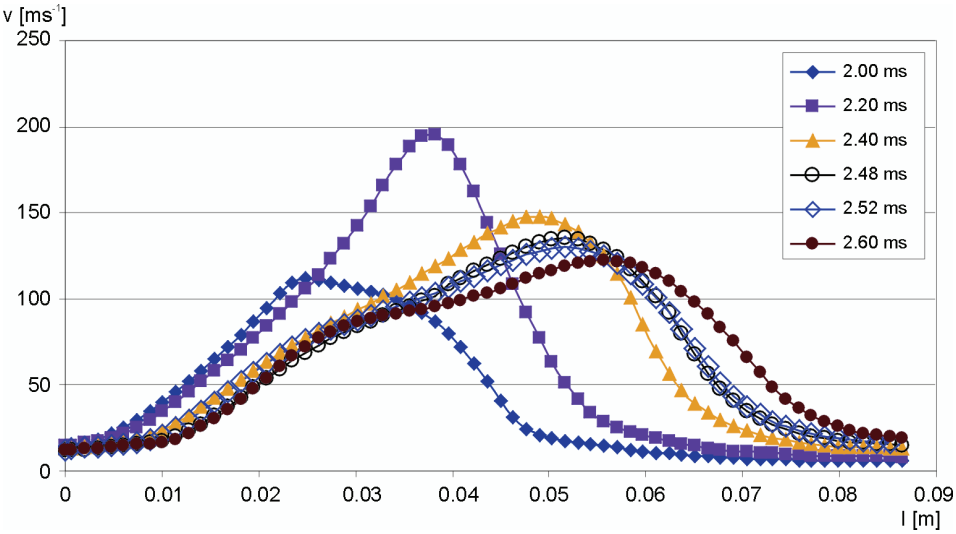

Fig. 4. Mass velocity distribution on the electrode arrangement model axis at time intervals from 2 ms to 2.60 ms

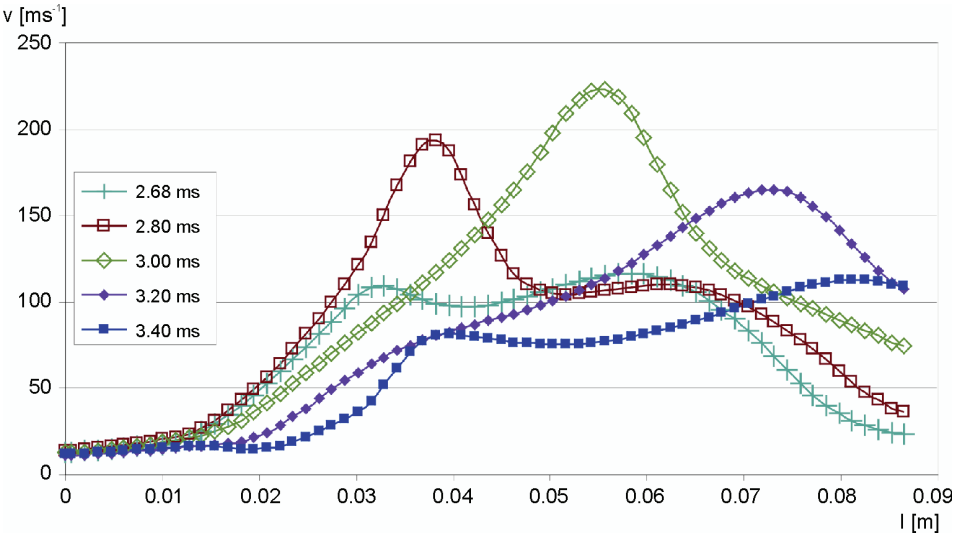

Fig. 5. Mass velocity distribution on the electrode arrangement model axis at time intervals from 2.68 ms to 3.40 ms

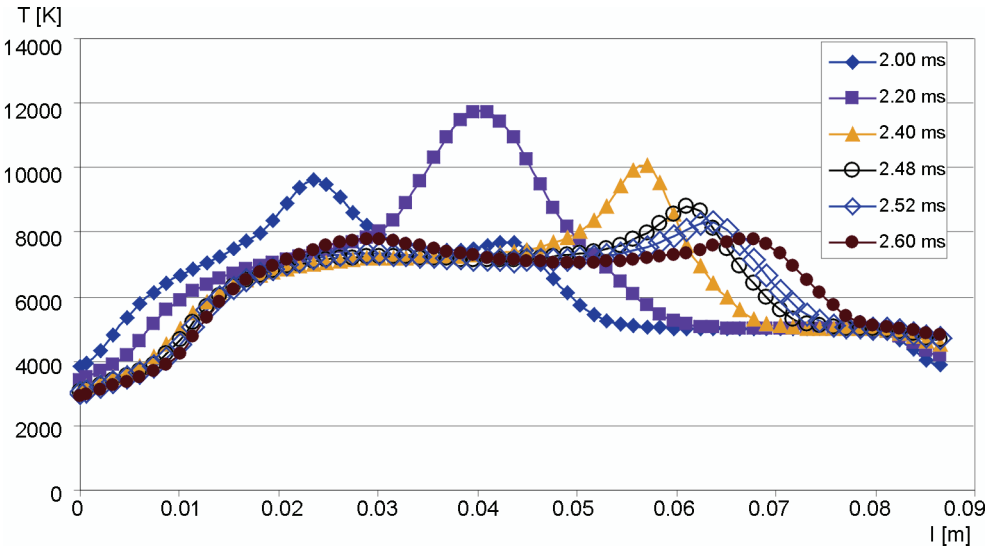

Fig. 6. Temperature distribution on the electrode arrangement model axis at time intervals from 2 ms to 2.60 ms

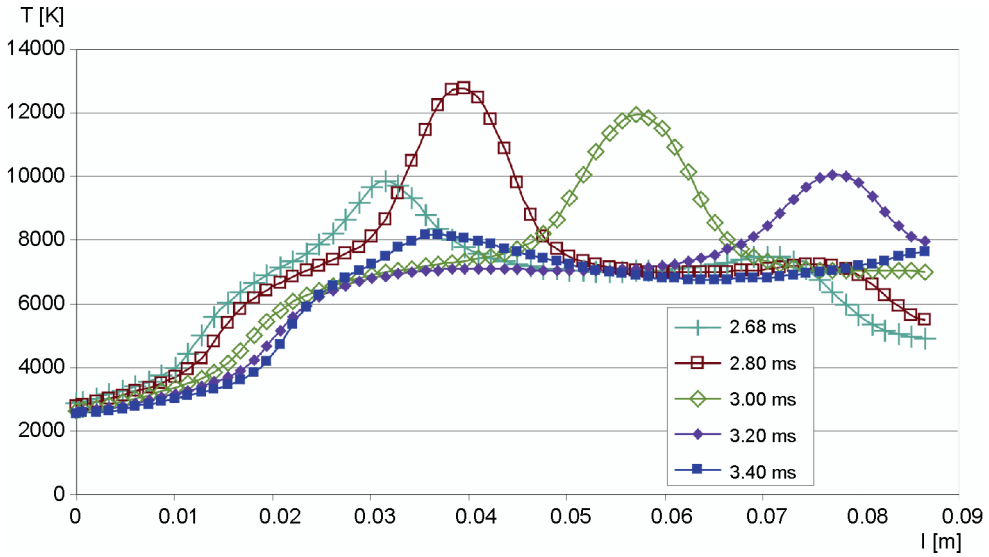

Fig. 7. Temperature distribution on the electrode arrangement model axis at time intervals from 2.68 ms to 3.40 ms

Then, although mass flow direction was not changed (Fig. 3), the new distributions of mass velocity values were formed for different instants (Figs. 4 and 5). The shapes of these distributions are very similar to those of temperature distributions (Figs. 6 and 7) and to current density distributions for different instants (Figs. 8 and 9). It results from the temperature distribution diagrams on the model axis that the temperature distributions vary in time from 2 ms to

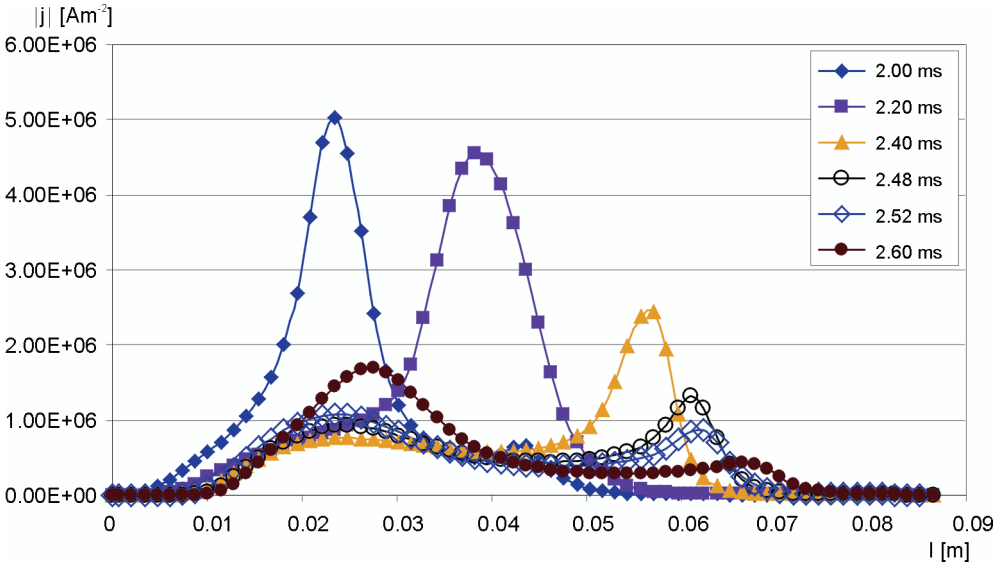

Fig. 8. Current density distribution on the electrode arrangement model axis at time intervals from 2 ms to 2.60 ms

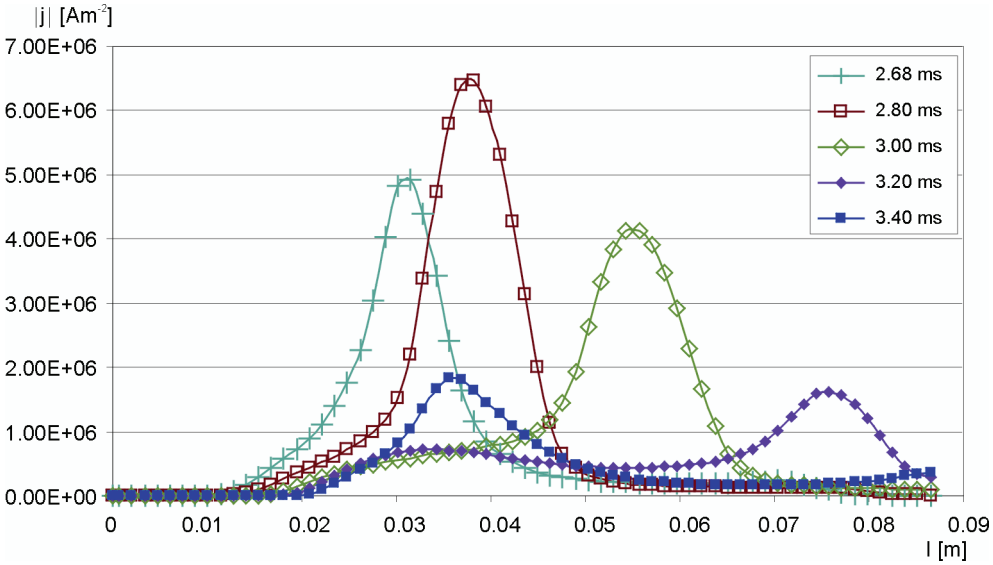

Fig. 9. Current density distribution on the electrode arrangement model axis at time intervals from 2.68 ms to 3.40 ms

3.40 ms in such a way that there is an impression of upward temperature cloud displacement over the model arrangement.

The first current density distribution of Fig. 8 (at 2 ms) is sharp in shape with a maximum density of about $5 \cdot 10^6$ A/m^2. With time, the channel with current increases its diameter and

moves upwards. The maximum current density slowly decreases and, at 2.40 ms, it is approximately $2.5 \cdot 10^6$ A/m^2, and at 2.48 ms ca $1.3 \cdot 10^6$ A/m^2. Next, from the time interval of 2.52 ms, when a new channel occurs and successively takes over the current (Figs. 8, 9), the maximum current density in the old channel drops down to $0.5 \cdot 10^6$ A/m^2 at the time interval of 2.60 ms. The phenomenon of the new channel appearance is repeated after the time interval of 3.20 ms somewhat higher than formerly (about 35 mm over the tips of electrodes), which results in formation of a new current density maximum in that particular location (Fig. 9).

Current density variations are correlated with temperature variations. It is evident from Figs. 6 and 7 that a new temperature maximum starts its formation between the instants of 2.52 ms and 2.68 ms about 30 mm above the tips of electrodes. It increases its value, attaining the maximum after 2.80 ms from the current zero passage after 8 mm displacement. One can correlate this phenomenon to the appearance of a new discharge channel, which takes over a current conduction, as Figs. 8 and 9 shows that the new current density maximum (10^6 A/m^2) appears at 2.52 ms time point at 25 mm over the tips of electrodes, attaining $1.73 \cdot 10^6$ A/m^2 at instant 2.6 ms, and $5 \cdot 10^6$ A/m^2 at instant 2.68 ms about 30 mm above the electrode tip.

4. Conclusions

The high spatial mobility of discharge channels in AC electric arcs, observed during the experiments and filmed at different planes, resulted in dynamic arc position changes [7, 8]. The plasma jets, coming off electrodes, run in different directions and the channel between them takes often twisted shapes, which makes the formation of new discharge channels much easier. The classical filming of arc with one camera will always provide simplified plain arc pictures. The phenomena at the plane of a photo are recorded, while the phenomena running at the plane, perpendicular to the filming plane, are not visible. In this respect, computer simulation is evidently much more efficient and generally more advantageous over the mere recording of phenomena with high-speed cameras to provide plane pictures only.

The images, obtained during arc simulation, can be viewed not only in space but also many plasma parameters can be analyzed, and not only the external parameters, related generally to geometrical aspects. The analyses of those parameters can be multi-sided as the distributions of particular quantities, as mentioned above, may be obtained at each discharge section. Such analyses, as presented here, were carried out with the use of state-of-the-art computer programs, designed and adapted for this particular purpose.

Beside the above-mentioned advantages of the presented arc simulation, some of its weaker points should also be remembered. Though the pictures of arc burning and of new discharge channel formation, obtained by computer simulations in the model arrangement of electrodes, were qualitatively similar to the pictures recorded with a Photron digital film camera [8], there were fairly large differences in the values of currents, at which the new discharge channels occurred. The cause of that situation will be searched for in subsequent research.

Finally, another other important problem will be considered, namely the arc motion, as investigated here, had for many been identified years with arc mass motion under the influ-

ence of buoyancy forces and the forces of electrodynamic interaction between the arc current and the internal or external magnetic field, and then the rod model of arc was assumed. The results, as presented here, show a correlation between mass velocity distribution displacement along the model axis in its actual arrangement and the temperature distribution displacement, but only in absence of jumps in discharge channel displacement. In the cases of complex switch arc motion (continuous and jumping motion), one should talk about matter state changes (e.g. thermal state).

Additionally, still another important aspect must be taken into account. Considering the fact that, for an external observer the electric arc is a luminous phenomenon, where temperature cloud is the source of light, the analysis resolves itself into calculations of the average values, when the same observer assumed the arc model in a form of a rod with definite dimensions (determined mostly from photographic observations) and mass. Such rod moves with an average velocity that is the same for each point of its structure. However, as it results from the simulation presented here, the arc motion should be considered as temperature distribution displacement. Then, each part of discharge can have a different velocity and only the average velocity of particular temperatures can be calculated. For instance, the average displacement velocity of a maximum temperature on the axis of the used electrode arrangement varied between the time intervals of 2.68 ms – 2.80 ms – 3.00 ms – 3.20 ms (Fig. 7) are 70 m/s – 90 m/s – 105 m/s respectively. The maximum mass velocity for those time intervals are: 116 m/s – 193 m/s – 223 m/s – 165 m/s, respectively.

Acknowledgment

This study, as a Research Project N N510 447536, was supported by the funds for science for the years 2009/2010. This is a continuation of the study, presented in the paper W. Tarczyński, T. Daszkiewicz, *Dynamics of discharge channel displacement in AC electric arcs.* Arch. of Electr. Eng. 58(3-4), 127-142 (2009) and supported likewise by the funds for science for the years 2009/2010 as the Research Project N N510 447536.

References

[1] Shanqiang Gu, Jinliang He, Bo Zhang et al. *Movement Simulation of Long Electric Arc Along the Surface of Insulator String in Free Air. IEEE Transactions on Magnetics* 42(4): 1359-1362 (2006).

[2] S. Tanaka, K. Sunabe, *Study on simple simulation model for dc free arc behavior in long gap*. Proc. 14th Int. Conf. Gas Discharges and Their Applications 1: 119-122 (2002).

[3] W. Tarczyński, *Kinetics of low-voltage switching arc*. Dissertations No. 225, Scientific Journals of Technical University of Lodz 746, 159 (1995).

[4] W. Tarczyński, *Electrodynamics of electrical apparatus. Publication series: Advances in High-Voltage Technique*. The Committee on Electrical Engineering of the Polish Academy of Sciences. Technical University of Lodz Publishers: 307, Łódź 2007.

[5] N.M. Schnurr, J.F. Kerrisk, J.V. Parker, *Numerical predictions of railgun performance including the effects of ablations and arc drag.* IEEE Transactions on Magnetics MAG-22 6: 1733 (1986).

[6] H.-G. Stäblein, *Arcs in cross flow.* Phenomena in Ionized Gases. Invited Lectures: 341-359, Berlin 1977.

[7] T. Daszkiewicz, *Analysis of dynamic states of discharge channels between plasma jets in AC electric arc*. Doctor's thesis. Department of Electrical Apparatus, Technical University of Lodz 2010.

[8] W. Tarczyński, T. Daszkiewicz, *Dynamics of discharge channel displacement in AC arcs.* Arch. of Electr. Eng. 58(3-4): 127-142 (2009).
[9] H.H. Maecker, *Principles of arc motion and displacement*. Proc. of the IEEE 59(4): 439-449 (1971).
[10] H.H. Maecker, *Motion of arcs*. Proc. of Int. Conf. on Phen. Ion. Gases.: 34-45, Mińsk 1981.
[11] H. Rachard, P. Chevrier, D. Henry, D. Jeandel, *Numerical study of coupled electromagnetic and aerothermodynamic phenomena in a circuit breaker electric arc*. International Journal of Heat and Mass Transfer 42: 1723-1734 (1999).
[12] F. Karreta, M. Lindmayer, *Simulation of arc motion under conditions of low voltage switchgear*. Proc. of the XII Int. Conf. on Gas Discharges and their Applications: I-135-I-138, Germany 1997.
[13] D. Bernardi, V. Colombo, E. Ghedini et al. *Three-Dimensional Time-Dependent Modeling of Magnetically Deflected Transferred Arc.* IEEE Transactions on Plasma Science 33(2): 428-429 (2005).
[14] J.-J. Gonzalez, P. Freton, A. Gleizes, *Theoretical study of hydrodynamic flow in thermal plasma devices.* Czechoslovak Journal of Physics 56(Suppl. B): B721-B732 (2006).
[15] X. Franceries, F. Lago, J.-J. Gonzalez et al. *3-D Visualization of a 3-D Free-Burning Arc Model Deflected by External Magnetic or Convective Forces*. IEEE Transactions on Plasma Science 33(2): 432-433 (2005).
[16] F. Lago, P. Freton, J.-J. Gonzalez, *Numerical Modeling of the Interaction Between an Electric Arc and a Material: Application to the Lightning Stroke of an Aircraft*. IEEE Transactions on Plasma Science 33(2): 434-435 (2005).
[17] Ch. Rümpler, F. Reichert, H. Stammberger, P. Terhoeven, F. Berger, *Numerical study of the electrical arc movement supported by experiments*. ICEC: 22-27 (2006).
[18] M. Masqu`ere, P. Freton, J.-J. Gonzalez, *Theoretical study in two dimensions of the energy transfer between an electric arc and an anode material*. J. Phys. D: Appl. Phys. 40: 432-446 (2007).
[19] X. Zhang, J. Zhang, E. Gockenbach, *Calculation of pressure and temperature in medium-voltage electrical installations due to fault arcs*. J. Phys. D: Appl. Phys. 41: 195-206 (2008).
[20] J. Heberlein, A.B. Murphy, *Thermal plasma waste treatment*. J. Phys. D: Appl. Phys. 41, 053001 (2008).
[21] E. Domejean, P. Chevrier, C. Fievet, P. Petit, *Arc-wall interaction modelling in a low-voltage circuit breaker.* J. Phys. D: Appl. Phys. 30: 2132-2142 (1997).
[22] J. Haidar, *Non-equilibrium modelling of transferred arcs*. J. Phys. D: Appl. Phys. 32: 263-272 (1999).
[23] M.A. Ramırez, G. Trapaga, J. McKelliget, *A comparison between two different numerical formulations of welding arc simulation*. Modelling Simul. Mater. Sci. Eng. 11: 675-695 (2003).
[24] X. Li, D. Chen, R. Dai, Y. Geng, *Study of the Influence of Arc Ignition Position on Arc Motion in Low-Voltage Circuit Breaker*. IEEE Transactions on Plasma Science 35(2) (2007).
[25] F. Reichert, F. Berger, Ch. Rumpler et al. *Experimental studies of the arc behaviour in low voltage arc rail arrangements supporting numerical simulations*. IEEE Holm Conference on Electrical Contacts: 34-39 (2006).
[26] S.V. Patankar, *Numerical Heat Transfer and Fluid Flow*. Series in Computational Methods in Mechanics and Thermal Science, New York, Hemisphere Publishing Corporation (1980).